# A non-dispersive infrared sensor for real-time detection of cyanogen chloride

**Bin Ma[a], Lijun Ren[a], Guohong Liu[a,b*], Jian Li[a], Yanhua Xiao[a], Danping Li[a], Ying Gao[b] and Peng Kuang[c]**

[a]*Department of Chemical Defense, Institute of NBC Defense, PLA Army, Beijing China.*
[b]*Unit 96901, PLA, Beijing China.*
[c]*Poly Group Beijing New Era global import and Export Co., Ltd, Beijing China.*

Received 03 March 2021, revised 24 December 2021, accepted 24 December 2021

**ABSTRACT**

**Cyanogen chloride, as a systemic toxic agent, can cause death rapidly. In this paper, a non-dispersive infrared sensor was designed for the infrared absorption detection of cyanogen chloride at 800 $cm^{-1}$. The roughness of the internal coating material was analyzed by experiments, and the gold-plated gas chamber was selected. The light path propagation of different cross-section gas chambers was simulated, and the circular section gas chamber was selected to increase the infrared detector signal. The effect of flow rate on voltage was studied. The standard curve between voltage and concentration was obtained under the optimal condition of 0.4 L $min^{-1}$. The maximum response time was 19 s, and RSD was less than 2%. The interference experiment results showed that common gases entering the gas chamber do not cause interference. The non-dispersive infrared sensor for cyanogen chloride has good stability and detects cyanogen chloride in real-time.**

**KEYWORDS**

**cyanogen chloride, NDIR, real-time, qualitative analysis, quantitative analysis**

## INTRODUCTION

Cyanogen chloride (CNCl) is an important chemical intermediate, widely used in pesticides, medicine, and chemical additives and was used as a systemic toxic agent in World War II. For example, CNCl is used to produce cyanuric chloride and the synthesis of tetramethyl guanidine.[1,2] CNCl has the characteristics of low boiling point and volatility and usually exists as a gas.[3,4] Cyanogen in CNCl has strong coordination ability. It can combine with the trivalent iron ion in cells, affecting normal respiration and causing asphyxia. After poisoning, people will have dizziness, nausea and vomiting; in severe cases, the body muscles will be paralyzed, and the reflex will be lost, resulting in death within a few minutes.[5-7] With the increase of storage capacity and types of hazardous chemicals year by year, safety issues should not be underestimated. The rapid and accurate detection of CNCl has become an indispensable requirement. Generally, gas detection methods mainly include ion chromatography,[8–10] catalytic combustion,[11,12] electrochemical methods,[13,14] and gas chromatography.[15–17] However, most detection devices on which these methods are based are expensive, inconvenient to carry and cannot detect CNCl in real-time.

Non-dispersive infrared (NDIR), as a real-time gas detection method, selects the specific infrared absorption as the basis of qualitative recognition and quantitative analysis. At present, NDIR sensors play an important role in coal mine safety, air detection, environmental management, and other fields,18-20 since they can detect $CO_2$, CO, NO, $NO_2$, $SO_2$, $CH_4$ $C_2H_5OH$, $C_2H_4$ and other inorganic and organic gases.[21-23] Barritault et al. report the fabrication and characterization of an NDIR sensor based on a micro-bolometer detector and a Micro-Electro-Mechanical System (MEMS) IR-source, which has a very low power consumption.[24] Gibson and Macgregor developed a new type of carbon dioxide NDIR sensor combined with a mid-infrared light-emitting diode light source and a photodiode detector.[25] The sensor has the advantages of fast stabilization time, low power consumption and low cost.[25] Tan et al. designed an NDIR device with a parabolic gas chamber where environmental temperature, humidity, and pressure changes are reduced through linear compensation.[26] Therefore, NDIR sensor detection methods have good poison detection and analysis prospects.

The purpose of this paper is to develop an NDIR sensor that qualitatively and quantitatively detects CNCl in real-time. In this work, the detection wavelength was selected according to the infrared spectrum. The appropriate components of the NDIR sensor are selected, and the roughness of the gas chamber with different coating materials is compared. The cross-section shape of the gas chamber is simulated and optimized. The effect of flow rate on the voltage response value of CNCl was studied. Under the optimal conditions, we obtained the standard curve and detection limit of CNCl gas. We tested the response time, precision and selectivity of the sensor through a series of experiments.

## MATERIALS AND METHODS

### Chemicals and reagents

The Institute of NBC Defense provided CNCl. Different concentrations of CNCl were prepared by the static gas distribution method. Firstly, the air in the gas bag was evacuated, and the quantitative gas tube absorbed a certain amount of CNCl gas and injected it into the gas bag. Then, nitrogen is slowly injected into the gas bag. Then the gas bag was squeezed several times, and the gas mixed evenly. The real concentration of CNCl in the gas bag was detected using a photoacoustic spectrometer.

Nitrogen ($N_2$), $CO_2$, CO, NO, $NO_2$, $N_2O$, $CH_4$, $SO_2$, $H_2$, $H_2S$, $O_2$, $NH_3$, $CH_4$, $C_2H_5OH$ and propane ($C_3H_8$) were provided by Beijing Zhaoge Gas Technology Co., Ltd.

### Instruments

In this investigation, a multimeter (Unitech (China) Co., Ltd), photoacoustic spectrometer (Institute of NBC Defense), optical profilometer (Shanghai Microspectrum company), and a self-made NDIR sensor (Institute of NBC Defense) were used. The length of the gas chamber was 130 mm, the filter was a narrow-band pass filter, and the infrared detector was a pyroelectric detector. Lithium tantalate was chosen as the pyroelectric crystal, which has a fast response speed and can work at both high and low frequencies.

A schematic diagram of the sensor is shown in Fig. 1. The principle of the NDIR sensor is that the infrared light source is not divided at first. When the infrared light passes through the gas to be measured,

*To whom correspondence should be addressed
Email: liugh01@163.com

ISSN 1996-840X Online / South African Chemical Institute / http://saci.co.za/journal

https://doi.org/10.17159/0379-4350/2022/v76a03

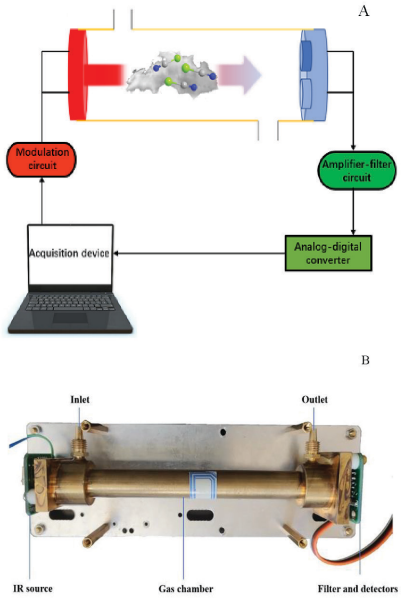


**Figure 1:** Schematic diagram A and physical picture B of CNCl NDIR sensor

a filter is used to let the infrared light of a specific wavelength pass through. The transmission wavelength of the filter is the selected detection wavelength. The infrared detector converts the optical signal into an electrical signal, and an amplification circuit amplifies the signal. The unknown gas concentration can be obtained according to the collected voltage value.

## METHODS

Different concentrations of CNCl were introduced into the gas chamber of the sensor. The positive and negative electrodes of the sensor were connected with a multimeter, and a computer collected the voltage response value.

For the quantitative detection in NDIR sensor, according to Lambert Beer's law:[27-30]

$$I = I_0 e^{-kcl} \quad (1)$$

$I_0$ represents the incident light intensity of the detection wavelength, I represents the outgoing light intensity of the detection wavelength, k is the gas absorption coefficient, c is the gas concentration, and l is the optical path. In the formula: $I \propto (1/c)$, the detector converts the optical signal into an electrical signal, and there are reference gas and detection gas in the gas chamber. Therefore:

$$U_{act} \propto I_{act}, U_{ref} \propto I_{ref} \quad (2)$$

$U_{act}$ $U_{ref}$ represents voltage signals of the CNCl channel and nitrogen channel, respectively. $I_{act}$ and $I_{ref}$ represent the incident light intensity of the CNCl channel and nitrogen channel, respectively. After introducing the parameters α, β, the following relation is obtained:

$$U_{act} = I_{act} e^{-kcl} a, U_{ref} = I_{ref} b \quad (3)$$

α represents the joint influence of the transmittance of the detection filter and the response constant of the poison detector, respectively. β is the joint effect of the reference filter's transmittance and the nitrogen detector's response constant. $U_{ref} - U_{act}$:

$$\Delta U = U_{ref} - U_{act} \propto c \quad (4)$$

It can be seen from the above formula that the difference between the reference voltage minus the measured voltage (ΔU) is proportional to the concentration c.

## RESULTS AND DISCUSSION

### Selection of wavelength

The molecular composition of CNCl is composed of three atoms. The $CN^-$ group has a strong electron absorption effect, which leads to the mismatch of positive and negative charge centres, so the dipole moment is not zero. When a molecule vibrates or rotates, the dipole moment changes. At this time, CNCl can absorb specific infrared radiation.

The infrared spectrum of CNCl was obtained by experiment, as shown in Figure 2. According to the results, the infrared peaks of high absorption intensity of CNCl are 320 $cm^{-1}$, 800 $cm^{-1}$ and 2300 $cm^{-1}$. As 320 $cm^{-1}$ does not belong to the mid-infrared region, it cannot be used as the detection wavelength. It was concluded that 2300 $cm^{-1}$ (4.3 μm) was the absorption peak of C≡N, but it is close to the beam of carbon dioxide in the air at 2300 $cm^{-1}$. Especially in the explosion environment, there will be a high concentration of $CO_2$, so the detection at this position will produce interference. 800 $cm^{-1}$ is the bending vibration of Cl≡C, and the absorption of the peak is high. The infrared absorption position of water vapour is around 1200–1900 $cm^{-1}$ and 3400–4000 $cm^{-1}$, so it will not result in interference. Other common gases in the air will not produce interference at 800 $cm^{-1}$. Therefore, 800 $cm^{-1}$ was selected as the infrared detection beam of CNCl.

### Optimization of the gas chamber

#### *Optimization of coating*

CNCl absorbs infrared light through the gas chamber. When the parallel beam propagates in the gas chamber, some infrared light will be reflected and refracted in the gas chamber. The rougher the gas chamber is, the more diffuse the reflection will be, which will lead to an increase in light loss. At present, there are two types of gas chamber coating: aluminium and gold coating.

The inner surface roughness of two kinds of gas chambers with different materials was measured using a 3D optical profilometer. As shown in Figure 3 and Figure **4**, the roughness of the gold plating chamber (0.269 μm) is better than that of the aluminium chamber (0.277 μm). In addition, the chemical properties of aluminium are very unstable, and the surface of the aluminium film will react with oxygen in the atmosphere to form alumina film, which will reduce the smoothness of the inner wall of the gas chamber. However, the gold plating chamber has better chemical stability, and exposure to CNCl gas will not be contaminated. Therefore, the gold plating chamber was selected as the best coating material.

#### *Section shape optimization*

The light intensity received by the infrared detector is affected by the cross-sectional shape of the gas chamber. The greater the light intensity received by the infrared detector, the higher the detection accuracy of

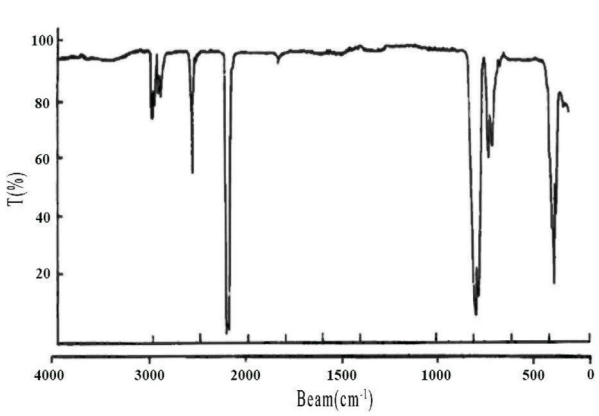


**Figure 2:** Experimental infrared spectrum of CNCl

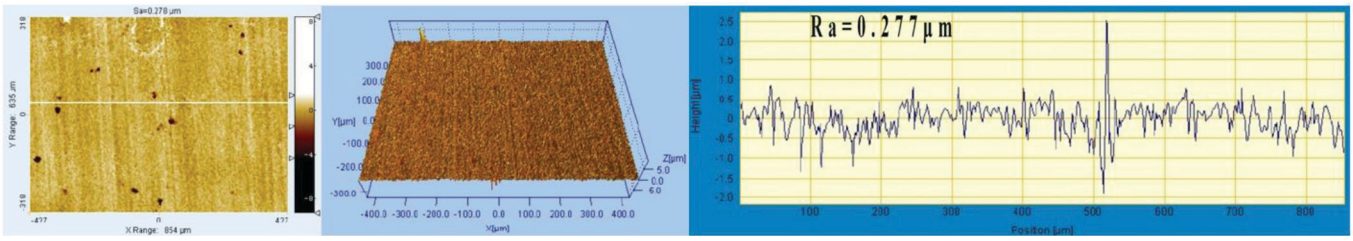


**Figure 3:** Internal roughness test diagram of the aluminium chamber

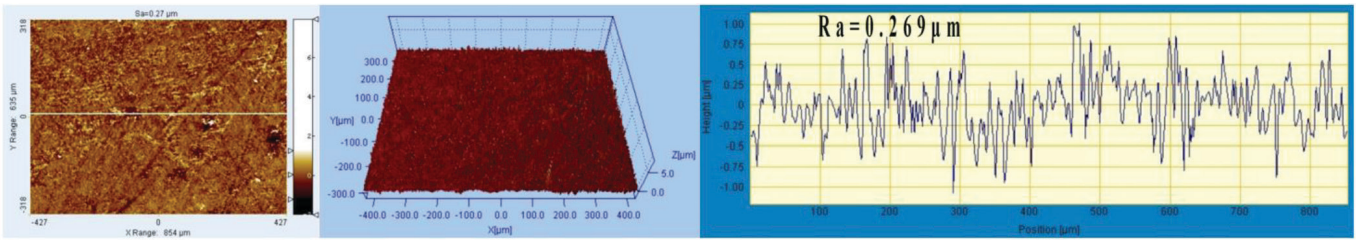


**Figure 4:** Internal roughness test diagram of the gold plating chamber

the instrument. The effect of circular and square configurations on the detection effect of the detector was simulated (Figs 5 and 6). The maximum irradiance of the square section gas chamber is 21 624 W $m^{-2}$, and that of the circular section gas chamber is 38 744 W $m^{-2}$. While for the average irradiance, the square section gas chamber is 11798 W $m^{-2}$ and the circular section gas chamber is 12 445 W $m^{-2}$. Therefore, under the same light source intensity, the light loss of the square section gas chamber was greater than that of the circular section gas chamber. In addition, because the detector detection channel is located in the central position and the light spot in the circular gas chamber is more concentrated, resulting in stronger optical signals and stronger output signals, the circular cross-section gas chamber should be selected for assembly.

## Effect of flow rate

In order to explore the effect of flow rate on voltage response, 3040 ppm CNCl was injected into the gas chamber at different flow rates, ranging between 0.4 and 0.65 L $min^{-1}$. The results of voltage acquisition are shown in Fig. 7. When the flow rate was less than 0.4 L $min^{-1}$, the voltage response value increased, but the curve slope gradually decreased. The voltage response value showed little change when the flow rate was greater than 0.4 L $min^{-1}$. Considering the power consumption of the sensor, the flow rate should not be too high. Therefore, a flow rate of 0.4 L $min^{-1}$ was selected as the optimal flow rate in the later experiments.

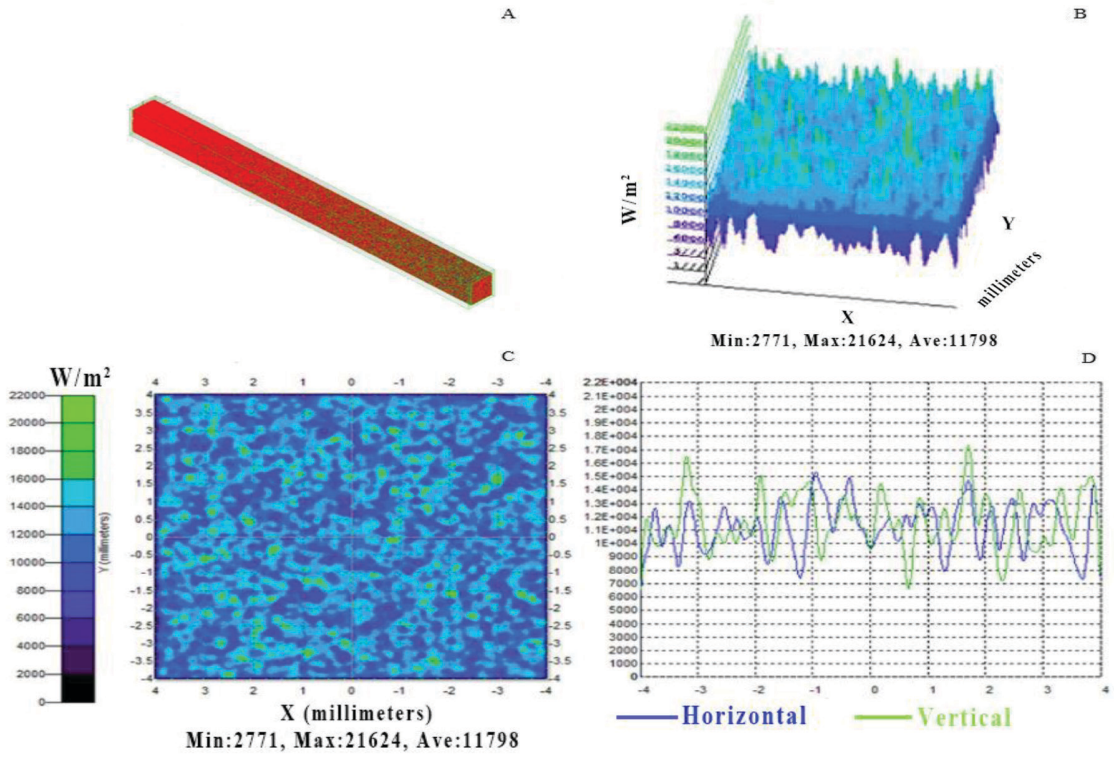


**Figure 5:** Simulation results of square section gas chamber. A is the structure diagram of the square cross-section gas chamber. The three-dimensional coordinate system is established with the centre of the infrared detector as the origin. The X and Y axes represent the position on the detector plane, and the Z-axis represents the irradiance. B represents the three-dimensional light intensity diagram of the detector after the infrared light passed through the gas chamber, C represents the vertical view light intensity distribution of the detector after the infrared light passed through the gas chamber. D represents the two-dimensional coordinate diagram of the light intensity distribution of the detector centre axis after the infrared light passes through the gas chamber.

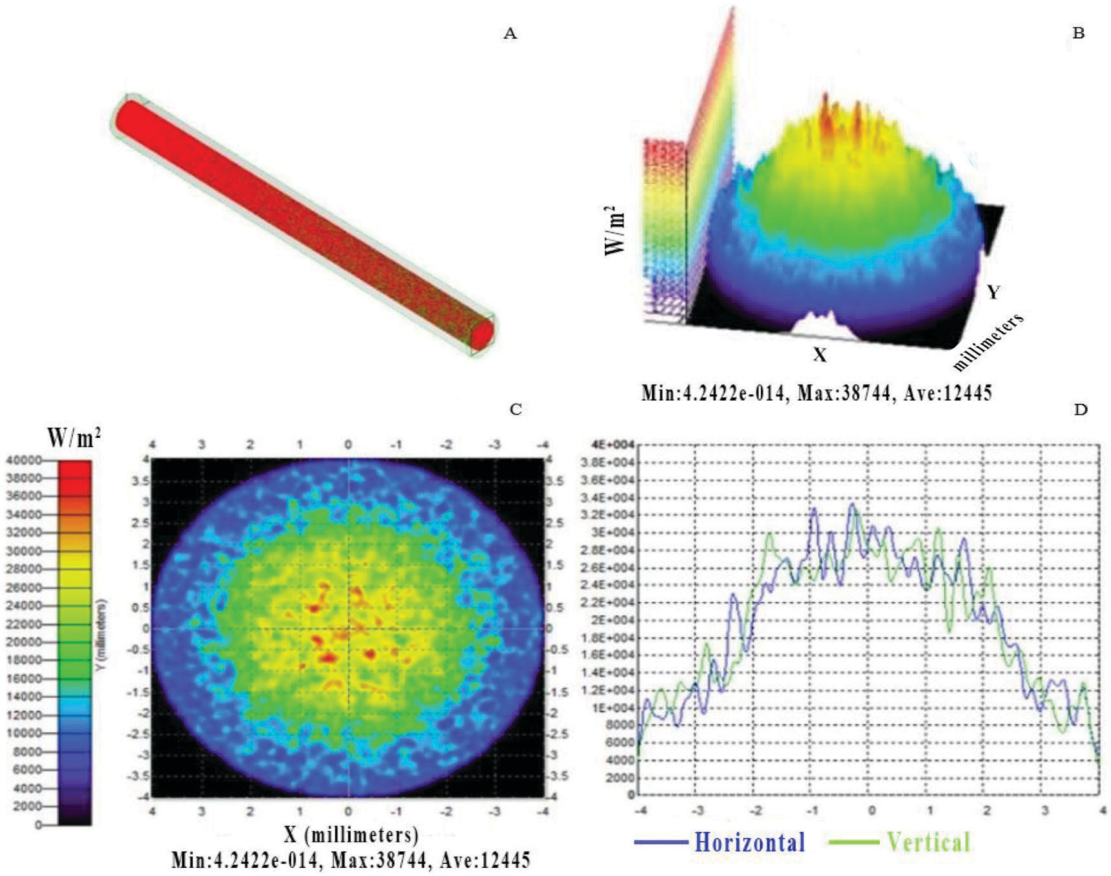


**Figure 6:** Simulation results of circular section gas chamber. A is the structure diagram of the circular cross-section gas chamber. The three-dimensional coordinate system is established with the centre of the infrared detector as the origin. The X and Y axes represent the position on the detector plane, and the Z-axis represents the irradiance. B represents the three-dimensional light intensity diagram of the detector after the infrared light passed through the gas chamber, C represents the vertical view light intensity distribution of the detector after the infrared light passed through the gas chamber. D represents the two-dimensional coordinate diagram of the light intensity distribution of the detector centre axis after the infrared light passes through the gas chamber.

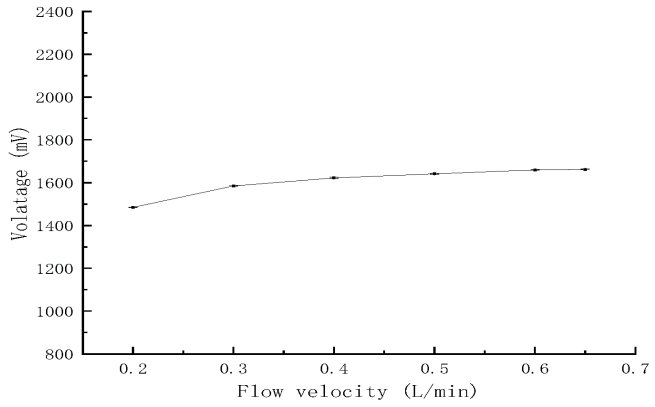


**Figure 7:** The effect of flow rate on the voltage at room temperature.

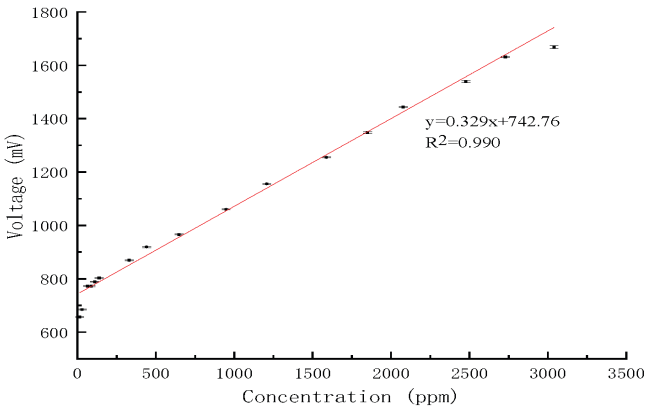


**Figure 8:** Voltage and concentration standard curve

## Analytical characteristics

### *Standard curve and precision experiment*

CNCl was prepared in a 1-L gas bag at room temperature and then introduced into the gas chamber. The gas concentration range for detection was 14–3040 ppm. The standard curve obtained between voltage and concentration was y = 0.329x + 742.76 with a linear range of 64 - 2730 ppm and a detection limit of 25 ppm (S/N = 3) (Fig. 8).

The CNCl standard gases of 330 ppm, 948 ppm, 1864 ppm and 2478 ppm were prepared in four 1-L gas bags by static gas distribution method, then the different concentrations of CNCl were introduced into the gas chamber. The experimental results are shown in Table 1. The relative standard deviations (RSD) of cyanide chloride concentrations measured were less than 0.5%.

### *Response time*

The response time of the instrument refers to the time required for a certain concentration of gas to reach 90% of the stable value from zero. Several gas bags were used to prepare CNCl with a concentration of 3040 ppm, 2400 ppm, 1864 ppm, 948 ppm, 625 ppm and 350 ppm. After each group of CNCl of different concentrations was passed into the gas chamber, the time required to reach 90% of the stable value was recorded. The maximum response time of the sensor is 19 s, which can achieve the real-time detection of CNCl (Fig. 9).

**Table 1:** The standard deviation and relative standard deviation of cyanogen chloride concentrations measured

| Actual conc. (ppm) | Measured conc. (ppm) | SD (ppm) | RSD (%) |
|---|---|---|---|
| 330 | 366 | 1.413 | 0.386 |
| 948 | 949 | 2.270 | 0.239 |
| 1864 | 1832 | 6.050 | 0.330 |
| 2478 | 2412 | 2.564 | 0.106 |

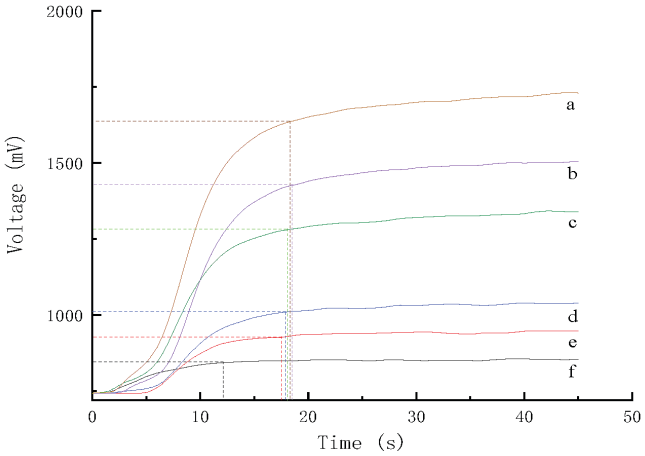


**Figure 9:** Response time of different concentrations. a, b, c, d, e and f denotes 3040 ppm, 2400 ppm, 1864 ppm, 948 ppm, 625 ppm and 350 ppm, respectively.

### *Selectivity*

At room temperature, we tested the interference performance of the sensor when different gases ($NH_3$, CO, $CO_2$, NO, $NO_2$, $N_2O$, $H_2S$, $H_2$, $O_2$, $SO_2$, He, $CH_4$, $C_3H_8$ and $C_2H_5OH$) pass through the CNCl sensor. After the sensor was preheated, gases of concentration 300 ppm were introduced into the chamber using a gas proportional pump, and the CNCl was continuously introduced into the gas chamber for 30 seconds. In the process of gas introduction, the results show that the concentration indication of the sensor is always 0 ppm. Hence, the CNCl NDIR sensor has good anti-interference performance for most common gases.

## CONCLUSIONS

In this project, the infrared absorption of CNCl at 800 $cm^{-1}$ was selected for detection wavelength. The circular gold plating chamber was selected to increase the light intensity received by the detector and the service life of the gas chamber. The standard curve between voltage and concentration is y = 0.329x+742.76 with the linear range of 64 - 2730 ppm and the detection limit of 25 ppm (S/N = 3). The maximum response time of the sensor was 19 s, which can realize the real-time detection of CNCl. Most common gases do not interfere with the CNCl NDIR sensor.

The NDIR sensor only needs to use the air pump to pump the external samples into the instrument and then detect them by non-dispersive infrared spectroscopy. No other consumables are needed. It has the characteristics of being easy to carry, offers real-time detection, long-life, good stability, and strong anti-interference ability. It has opened up a new field of non-dispersive infrared detection in toxic agents.

## Acknowledgements

This work is supported by the National key R&D project (2017YFA0207102) and the National key R&D project (2019YFC1200603).

## ORCID IDS

Bin Ma – https://orcid.org/0000-0002-2079-7294
Lijun Ren – https://orcid.org/0000-0002-6488-703X
Guohong Liu – https://orcid.org/0000-0001-7564-2305
Jian Li – https://orcid.org/0000-0002-9620-378X
Yanhua Xiao – https://orcid.org/0000-0003-4054-6764
Danping Li – https://orcid.org/0000-0003-3707-5789
Ying Gao – https://orcid.org/0000-0003-3681-8843
Peng Kuang – https://orcid.org/0000-0002-8086-6060

## REFERENCES

1. Webster OW. Polycyanation. The reaction of cyanogen chloride, cyclopentadiene, and sodium hydride. J Am Chem Soc. 1966;88(13):3046–3050. https://doi.org/10.1021/ja00965a028.
2. Vereshchagin LI, Verkhozina ON, Pokatilov FA, Proidakov AG, Kizhnyaev VN. Synthesis of polynuclear heterocyclic polynitrogen systems based on cyanuric chloride and its derivatives. Chem Heterocycl Compd. 2010;46(2):206–211. https://doi.org/10.1007/s10593-010-0493-2.
3. Na C, Olson TM. Stability of cyanogen chloride in the presence of free chlorine and monochloramine. Environ Sci Technol. 2004 Nov 15;38(22):6037–6043. https://doi.org/10.1021/es0498235.
4. Lee JH, Na C, Ramirez RL, Olson TM. Cyanogen chloride precursor analysis in chlorinated river water. Environ Sci Technol. 2006 Mar 1;40(5):1478–1484. https://doi.org/10.1021/es051409x.
5. Barnir Z, Aharoni C. Adsorption of cyanogen chloride on impregnated active carbon. Carbon. 1975;13(5):363–366. https://doi.org/10.1016/0008-6223(75)90003-2.
6. Reucroft PJ, Chiou CT. Adsorption of cyanogen chloride and hydrogen cyanide by activated and impregnated carbons. Carbon. 1977;15(5):285–290. https://doi.org/10.1016/0008-6223(77)90031-8.
7. Henderson TJ, Cullinan DB. Purity analysis of hydrogen cyanide, cyanogen chloride and phosgene by quantitative (13)C NMR spectroscopy. Magn Reson Chem. 2007 Nov;45(11):954–961. https://doi.org/10.1002/mrc.2081.
8. Inoue Y, Suzuki Y, Ando M. Determination of cyanide ion and cyanogen chloride by using photometric detection with 4-pyridinecarboxylic acid-pyrazolone in ion-exclusion chromatography. Bunseki Kagaku. 1993;42(10):617–623. https://doi.org/10.2116/bunsekikagaku.42.10_617.
9. Li H, Nonomura M, Itoh N. Simultaneous determination of residual chlorine and other anions in water by ion chromatography. Bunseki Kagaku. 2003;52:219–224.
10. Cui S, Kook KC, Kyoung-Seok L, Min HS. Study on the analytical method of arsenic species in marine samples by ion chromatography coupled with mass spectrometry. Microchem J. 2018;143:16–20. https://doi.org/10.1016/j.microc.2018.07.025.
11. Rodlamul P, Tamura S, Imanaka N. Effect of p- or n-type semiconductor on co sensing performance of catalytic combustion-type co gas sensor with $CeO_2$ -$ZrO_2$ -ZnO based catalyst. Bull Chem Soc Jpn. 2019;92(3):585–591. https://doi.org/10.1246/bcsj.20180284.
12. Gao Y, Wang S, Lv LR, Li DY, Wang SD. Insights into the behaviors of the catalytic combustion of propane over spinel catalysts. Catal Lett. 2020;150(12):3617–3625. https://doi.org/10.1007/s10562-020-03239-3.
13. Jovanovič P, Stojanovski K, Bele M, Dražić G, Koderman Podboršek G, Suhadolnik L, Gaberšček M, Hodnik N. Methodology for investigating electrochemical gas evolution reactions: floating electrode as a means for effective gas bubble removal. Anal Chem. 2019 Aug 20;91(16):10353–10356. https://doi.org/10.1021/acs.analchem.9b01317.
14. Touny AH, Saleh MM, El-Lateef HMA, Saleh MM. Electrochemical methods for fabrication of polymers/calcium phosphates nanocomposites as hard tissue implants. Appl Phys Rev. 2019;6(2):6–19. https://doi.org/10.1063/1.5045339.
15. Das P, Gupta M, Jain A, Verma KK. Single drop microextraction or solid phase microextraction-gas chromatography-mass spectrometry for the determination of iodine in pharmaceuticals, iodized salt, milk powder and vegetables involving conversion into 4-iodo-N,N-dimethylaniline. J Chromatogr A. 2004 Jan 9;1023(1):33–39. https://doi.org/10.1016/j.chroma.2003.09.056.
16. Yuan Z, Bariya M, Fahad HM, Wu J, Han R, Gupta N, Javey A. Trace-Level, Multi-Gas Detection for Food Quality Assessment Based on Decorated

Silicon Transistor Arrays. Adv Mater. 2020 May;32(21):e1908385. https://doi.org/10.1002/adma.201908385.

17. Xiang Z, Chen X, Qian C, He K, Xue X. Determination of volatile flavors in fresh navel orange by multidimensional gas chromatography quadrupole time-of-flight mass spectrometry. Anal Lett. 2020;53(4):614–626. https://doi.org/10.1080/00032719.2019.1662429.
18. Pellikka T, Kajolinna T, Perälä M. $SO_2$ emission measurement with the European standard reference method, EN 14791, and alternative methods - observations from laboratory and field studies. J Air Waste Manag Assoc. 2019 Sep;69(9):1122–1131. https://doi.org/10.1080/10962247.2019.1640809.
19. Moumen S, Raible I, Krauss A, Woellenstein J. Infrared investigation of $CO_2$ sorption by amine based materials for the development of a NDIR $CO_2$ sensor. Sens Actuators B Chem. 2016;236:1083–1090. https://doi.org/10.1016/j.snb.2016.06.014.
20. Dinh T, Ahn J, Choi I, Song K, Chung C, Kim J. Limitations of gas filter correlation: A case study on carbon monoxide non-dispersive infrared analyzer. Sens Actuators B Chem. 2017;243:684–689. https://doi.org/10.1016/j.snb.2016.12.036.
21. Gibson D, MacGregor C. A novel solid state non-dispersive infrared $CO_2$ gas sensor compatible with wireless and portable deployment. Sensors (Basel). 2013 May 29;13(6):7079–7103. https://doi.org/10.3390/s130607079.
22. Kosse P, Kleeberg T, Lübken M, Matschullat J, Wichern M. Quantifying direct carbon dioxide emissions from wastewater treatment units by nondispersive infrared sensor (NDIR) - A pilot study. Sci Total Environ. 2018 Aug 15;633:140–144. https://doi.org/10.1016/j.scitotenv.2018.03.174.
23. Vafaei M, Amini A, Siadatan A. Breakthrough in $CO_2$ measurement with a chamberless NDIR optical gas sensor. IEEE Trans Instrum Meas. 2019;9:1–15.
24. Barritault P, Brun M, Lartigue O, Willemin J, Ouvrier-Buffet J, Pocas S, Nicoletti S. Low power $CO_2$ NDIR sensing using a micro-bolometer detector and a micro-hotplate IR-source. Sens Actuators B Chem. 2013;182:565–570. https://doi.org/10.1016/j.snb.2013.03.048.
25. Gibson D, MacGregor C. A novel solid state non-dispersive infrared $CO_2$ gas sensor compatible with wireless and portable deployment. Sensors (Basel). 2013 May 29;13(6):7079–7103. https://doi.org/10.3390/s130607079.
26. Tan Q, Tang L, Yang M, Xue C, Zhang W, Liu J, Xiong J. Three-gas detection system with IR optical sensor based on NDIR technology. Opt Lasers Eng. 2015;74:103–108. https://doi.org/10.1016/j.optlaseng.2015.05.007.
27. Rose HE; Rose and E. H. Breakdown of the Lambert-Beer Law. Nature. 1952;169(4294):287–288. https://doi.org/10.1038/169287a0.
28. Stavn RH. Lambert-Beer law in ocean waters: optical properties of water and of dissolved/suspended material, optical energy budgets. Appl Opt. 1988 Jan 15;27(2):222–231. https://doi.org/10.1364/AO.27.000222.
29. Martin RL, Thomas BW. Infrared gas analyzer for butane splitter control. Ind Eng Chem Res. 2002;46:49–52. https://doi.org/10.1021/ie50535a922.
30. Ren LJ, Ma B, Liu GH, Li J, Xiao Y, Li D, Liu M, Gao Y, Kuang P. A portable NDIR sensor for rapid detection of hydrogen cyanide in environment. IOP Conf Ser Earth Environ Sci. 2021;621(1):1–7. https://doi.org/10.1088/1755–1315/621/1/012121.